Theoretical and experimental analysis of channel mismatch in time-wavelength interleaved optical clock based on mode-locked laser

Guang Yang, Weiwen Zou,* Xing Li, and Jianping Chen

State Key Laboratory of Advanced Optical Communication Systems and Networks, Department of Electronic Engineering, Shanghai Jiao Tong University, Shanghai 200240, China
*wzou@sjtu.edu.cn

Abstract: We demonstrate a theoretical model of channel mismatch effect in a mode-locked laser based time-wavelength interleaved optical clock generation system. The channel mismatch effect includes clock timing mismatch, amplitude mismatch, and pulse shape mismatch. An explicit expression of this model is derived for 2-channel simple system and a numerical simulation of multiple-channel complicated system is carried out. In comparison with the experimental measurement, the feasibility of the theoretical model is verified for calibration and compensation of the channel mismatches.

©2015 Optical Society of America

OCIS codes: (060.5625) Radio frequency photonics; (230.0250) Optoelectronics; (250.4745) Optical processing devices; (000.4430) Numerical approximation and analysis.

References and links

1. G. C. Valley, "Photonic analog-to-digital converters," Opt. Express **15**(5), 1955–1982 (2007).
2. J. Azaña and M. A. Muriel, "Temporal self-imaging effects: theory and application for multiplying pulse repetition rates," IEEE J. Sel. Top. Quantum Electron. **7**(4), 728–744 (2001).
3. T. R. Clark, J. U. Kang, and R. D. Esman, "Performance of a time- and wavelength-interleaved photonic sampler for analog-digital conversion," IEEE Photon. Technol. Lett. **11**(9), 1168–1170 (1999).
4. A. Yariv and R. G. M. P. Koumans, "Time interleaved optical sampling for ultra-high speed A/D conversion," Electron. Lett. **34**(21), 2012–2013 (1998).
5. A. Khilo, S. J. Spector, M. E. Grein, A. H. Nejadmalayeri, C. W. Holzwarth, M. Y. Sander, M. S. Dahlem, M. Y. Peng, M. W. Geis, N. A. DiLello, J. U. Yoon, A. Motamedi, J. S. Orcutt, J. P. Wang, C. M. Sorace-Agaskar, M. A. Popović, J. Sun, G. R. Zhou, H. Byun, J. Chen, J. L. Hoyt, H. I. Smith, R. J. Ram, M. Perrott, T. M. Lyszczarz, E. P. Ippen, and F. X. Kärtner, "Photonic ADC: overcoming the bottleneck of electronic jitter," Opt. Express **20**(4), 4454–4469 (2012).
6. X. Fu, H. Zhang, Y. Peng, and M. Yao, "40-Gbps time-and wavelength-interleaved pulse-train generation in wavelength-demultiplexing analog-to-digital conversion," Opt. Eng. **48**(10), 104302 (2009).
7. K. L. Lee, C. Shu, and H. F. Liu, "10 Gsample/s photonic analog-to-digital converter constructed using 10-wavelength jitter-suppressed sampling pulses from a self-seeded laser diode," CLEO 2001, pp. 67–68.
8. G. Wu, S. Li, X. Li, and J. Chen, "18 wavelengths 83.9Gs/s optical sampling clock for photonic A/D converters," Opt. Express **18**(20), 21162–21168 (2010).
9. N. Kurosawa, H. Kobayashi, K. Maruyama, H. Sugawara, and K. Kobayashi, "Explicit analysis of channel mismatch effects in time-interleaved ADC systems," IEEE Trans. Circuits Syst. I, Fundam. Theory Appl. **48**(3), 261–271 (2001).
10. C. Vogel, "The impact of combined channel mismatch effects in time-interleaved ADCs," IEEE Trans. Instrum. Meas. **54**(1), 415–427 (2005).
11. R. C. Williamson, P. W. Juodawlkis, J. L. Wasserman, G. E. Betts, and J. C. Twichell, "Effects of crosstalk in demultiplexers for photonic analog-to-digital converters," J. Lightwave Technol. **19**(2), 230–236 (2001).

1. Introduction

Photonic analog to digital conversion (PADC) technologies are developing rapidly in recent decades, aiming to overcome the limitation in electronic ADC (EADC) for high speed applications [1]. One of the crucial issues is the generation of a high quality optical sampling clock [2–5]. Several methods to multiply the repetition rate of the laser source, such as time

domain Talbot effect [2], time-wavelength interleaving [3, 4] etc., have been proposed for sampling clock generation. Time-wavelength interleaving method is more feasible and effective methods since it fully adopts the stability (i.e. low timing jitter) and ultrabroad spectral bandwidth (i.e. ultrashort pulse duration) of a mode-locked laser. Up to date, there are three typical ways to implement time-wavelength interleaving: multiple lasers with different wavelengths [6], multiple wavelength laser [7], and spectral slicing of a single broadband mode locked laser [5, 8]. In comparison, the spectral slicing method can generate a time-wavelength interleaved optical clock with higher speed and more feasibility [5]. An explicit analysis of channel mismatch effects has been proposed for time interleaved EADCs [9, 10], which is a good basis for the channel mismatch analysis in time-wavelength interleaved PADCs. A mathematical model for channel mismatch effects in time-wavelength interleaved PADCs was demonstrated [11]. However, in [11], the significant differences between PADCs and EADCs are not taken into account in the rather simple model and there is no corresponding experimental study and compensation method.

An effective analysis of channel mismatch effects in a mode locked laser based time-wavelength interleaved PADC should be based on its characteristics. Although the pulse trains in multiple channels are derived from the same laser with strict coherence, there are always differences in pulse trains among multiple channels since the laser's spectrum cannot be completely flat and there are phase (i.e. time delay or clock timing) fluctuation and amplitude mismatch among all the channels. Therefore, the mismatches of clock timing, amplitude, and pulse shape in time-wavelength interleaved PADC clock generation should be simultaneously considered. The mismatches of clock timing and amplitude are similar with those of EADCs, but the pulse shape mismatch is a distinctive characteristic in PADCs. Generally, an ultrahigh speed and high-cost oscilloscope laid after an ultrafast photo-detector is used to measure the temporal waveform of the PADC clock so as to characterize channel mismatch effects. For an ultrahigh speed PADC optical clock, temporal measurement becomes difficult due to the limitation of the sampling rate and/or bandwidth of the commercial oscilloscope.

In this paper, we propose a frequency domain method for characterization and compensation of the time-wavelength interleaved ultrahigh speed PADC clock generated from a mode locked laser. Based on the characteristics of mode locked laser based time-wavelength interleaved PADC, a theoretical analysis is carried out to study the impact of channel mismatch effects on time-wavelength interleaved clock generation. The mismatch of amplitude and pulse shape are analyzed directly from the optical frequency-domain measurement. Since the pulse shape mismatch is taken into account, this method provides a more precise analysis than the model proposed in [11]. Moreover, taking into account the ultrahigh sampling rate of PADC, the clock timing mismatch is analyzed through a frequency domain algorithm which is based on the prior analysis of amplitude and pulse shape mismatch. An analytical model of the relation between spectrum measurement and channel mismatch effects is established and an explicit expression is derived from this model for a simple 2-channel case. The multiple-channel numerical simulation is compared with the experimental measurement. Well consistence is obtained, verifying the effectiveness of the frequency domain method.

2. Principles

2.1. Generation and characterization of time-wavelength interleaved clock

Figure 1(a) shows a typical experiment configuration of time-wavelength interleaved clock generation with repetition rate of f_s. The spectrum of a mode locked laser with repetition rate at f_s/M is sliced into M channels via a wavelength division de-multiplexer (DMUX). An optical tunable delay line (TDL) and a variable optical attenuator (VOA) are connected into each channel to adjust the time delay and amplitude of the pulse train in each channel and

map the pulse trains in time domain. The pulse trains in all M channels are combined by a wavelength division multiplexer (WDM) to generate a time-wavelength interleaved clock with a repetition rate of f_s. A schematic of spectral slicing of mode locked laser and time-wavelength mapping of pulse trains in M channels is illustrated in Fig. 1(b). In mathematics, the intensity of optical pulse train in each channel can be expressed as

$$I_k(t) = a_k u_k(t - \tau_k) * \sum_{m=-\infty}^{+\infty} \delta\left[t - mMT_s - (k-1)T_s\right] \qquad k = 1, 2, \cdots, M, \qquad (1)$$

where τ_k, a_k, and $u_k(t)$ are the time skew (i.e. clock timing mismatch physically equivalent to phase mismatch), amplitude, and normalized intensity temporal pulse shape in the kth channel, respectively. $T_s = 1/f_s$ is the sample interval of the generated clock.
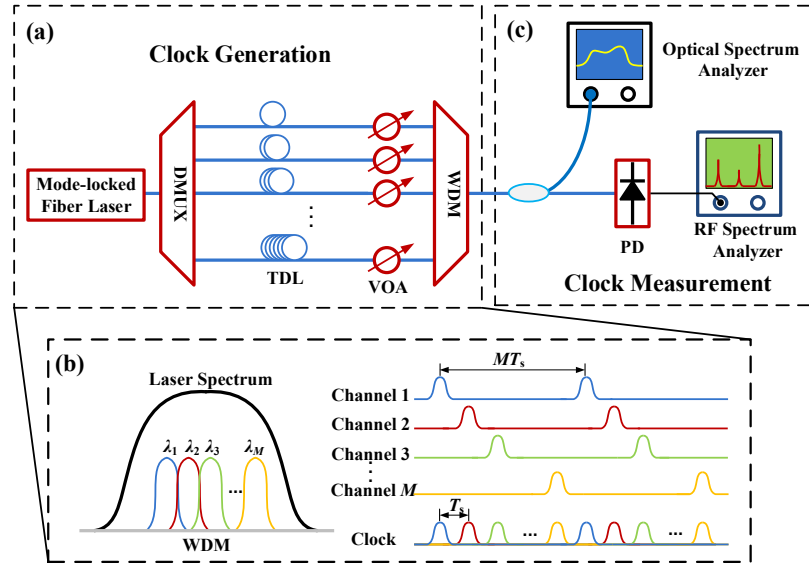

Fig. 1. (a) Experimental configuration of time-wavelength interleaved optical clock generation based on mode locked laser. (b) Schematic of spectral slicing of mode locked laser and time-wavelength mapping of pulse trains, (c) A frequency domain measurement method. DMUX: de-multiplexer, TDL: tunable delay line, VOA: variable optical attenuator, WDM: wavelength division multiplexer, PD: photo-detector.

In order to characterize the high-speed PADC clock, we propose a simple method as shown in Fig. 1(c). The optical spectrum of the clock is measured by an optical spectrum analyzer and the clock is converted into RF signal by a photo-detector (PD) for the RF spectrum measurement. The RF signal after the PD can be expressed as

$$s(t) = R_{PD} \sum_{k=1}^{M} I_k(t), \qquad (2)$$

where R_{PD} is the responsivity of the PD and the bandwidth of the PD is supposed to be sufficiently broad to obtain the response from $f = 0$ to the fundamental harmonic of $f = f_s$. The measured RF spectrum is given by

$$E(f) = \left|\tilde{S}(f)\right|^2 = \left|\frac{R_{PD}}{MT_s} \sum_{k=1}^{M} a_k \tilde{u}_k(f) e^{-j2\pi f \tau_k} e^{-j2\pi(k-1)f/f_s}\right|^2 \sum_{m=-\infty}^{+\infty} \delta(f - mf_s/M), \quad (3)$$

where $\tilde{S}(f)$ and $\tilde{u}_k(f)$ are the Fourier transform of $s(t)$ and $u_k(t)$, respectively.

2.2. Spectrum extinction ratio

For an ideal time-wavelength interleaved clock, the pulse train in each channel is identical, which can be denoted as $\tau_k = 0$, $a_k = a_0$, and $u_k(t) = u_0(t)$. Its RF spectrum can be correspondingly expressed as

$$E(f) = \left| \frac{R_{\mathrm{PD}}}{T_s} a_0 \tilde{u}_0(f) \right|^2 \sum_{m=-\infty}^{+\infty} \delta(f - m f_s). \tag{4}$$

Comparing Eq. (4) with Eq. (3), the impact of channel mismatch effects leads to the noise peaks at $f = k f_s/M$ ($k = 1,2,3,\ldots M-1$) in the RF spectrum as schematically illustrated in Fig. 2. The RF spectrum characteristics of the PADC clock with channel mismatch effects can be extracted from the peaks in $[0, f_s]$ as

$$E_k = E(k f_s/M) = \left(\frac{R_{\mathrm{PD}}}{M T_s} \right)^2 \left| \sum_{l=1}^{M} a_l \tilde{u}_l(k f_s/M) e^{-j 2\pi (k f_s/M)\tau_l} e^{-j 2\pi k(l-1)/M} \right|^2 \qquad k = 1, 2, \cdots, M.$$

$$\tag{5}$$

We define the spectrum extinction ratio η of the optical clock in the RF domain as the ratio between the power at the fundamental harmonic of $f = f_s$ and that of the noise peaks

$$\eta = 10 \log_{10}(E_s/E_n), \tag{6}$$

where E_s and E_n are given by

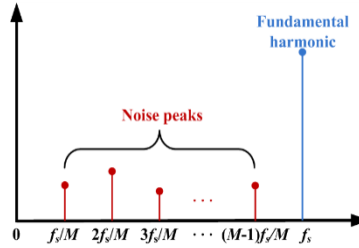$$E_n = \sum_{k=1}^{M-1} E_k, \quad E_s = E_M. \tag{7}$$

Fig. 2. Schematic of the PADC clock in RF domain.

3. Mathematical analysis

3.1 Mismatch parameters

For clock timing mismatch and amplitude mismatch, the time skews and amplitude in each channel can be normalized as follows

$$\hat{\tau}_k = (\tau_k - \bar{\tau})/T_s, \hat{a}_k = (a_k - \bar{a})/\bar{a}, \tag{8}$$

where $\bar{\tau}$ and $\bar{a}$ are the average of time skew and amplitude in each channel, respectively. The standard deviations of $\hat{\tau}$ and $\hat{a}$ are determined by

$$\sigma(\hat{\tau}) = \sigma(\tau)/T_s, \quad \sigma(\hat{a}) = \sigma(a)/\bar{a}, \tag{9}$$

where $\sigma(\cdot)$ represents the standard deviation. Equation (9) shows that the standard deviation of $\sigma(\hat{\tau})$ and $\sigma(\hat{a})$ correspond to the relative fluctuation of clock timing and amplitude among M channels, respectively.

Since the optical pulse in each channel are generated by spectrum slicing, the pulse shape in each channel cannot be well described by the most often used Gaussian or Sech^2 profile. Besides, the spectrum width of each spliced channel is always much larger than sampling rate, an effective approximation around $f = f_s$ via a Taylor expansion is reasonable to characterize the pulse shape mismatch effect. Hence a Lorentz approximation as derived in Appendix 1 is applied to $\tilde{u}_k(f)$ as follows.

$$\tilde{u}_k(f) \propto 1 \Big/ \Big[1 + \big(f/f_{c,k}\big)^2\Big], \quad f_{c,k}^2 = \Big[\delta(1/\tilde{u}_k)\Big/\delta\big(f^2\big)\Big]^{-1}\Big|_{f=f_s} = -2f_s\tilde{u}_k^2(f_s)\big/\tilde{u}_k'(f_s), \quad (10)$$

where $f_{c,k}$ is defined as the cutoff frequency of the kth channel. Similar to Eqs. (8) and (9), the normalized cutoff frequency $f_{c,k}$ and its deviation are derived as follows

$$\hat{f}_k = \big(f_{c,k} - \overline{f}_c\big)\big/\overline{f}_c, \quad \sigma\big(\hat{f}\big) = \sigma\big(f_c\big)\big/\overline{f}_c, \quad (11)$$

where $\overline{f}_c$ is the average of cutoff frequencies in each channel. Another parameter is defined as the normalized frequency ratio ρ between the sampling rate and the average cutoff frequency

$$\rho = f_s\big/\overline{f}_c. \quad (12)$$

3.2. Analytical model

Substitute Eqs. (8), (11), and (12) into Eq. (5), the spectrum peaks E_k for $k = 1,2,\ldots,M$ are derived as multivariate functions of the normalized time skew $\hat{\tau}$, the normalized amplitude $\hat{a}$, the normalized cutoff frequency $\hat{f}$ and the normalized frequency ratio ρ as follows

$$E_k\big(\hat{\tau},\hat{a};\hat{f},\rho\big) = \big(R_{PD}\overline{a}/MT_s\big)^2 \sum_{l,m=1}^{M} u_k\big(\hat{f}_l,\rho\big)u_k\big(\hat{f}_m,\rho\big)(1+\hat{a}_l)(1+\hat{a}_m)\cos\frac{2\pi k}{M}\Big[(\hat{\tau}_l - \hat{\tau}_m)+(l-m)\Big],$$

$$(13)$$

where $u_k\big(\hat{f},\rho\big) = 1\Big/\Big[1+k^2\rho^2/M^2\big(1+\hat{f}\big)^2\Big]$. Hence, the spectrum extinction ratio η can be expressed as a multivariate function

$$\eta\big(\hat{\tau},\hat{a};\hat{f},\rho\big) = 10\log_{10}\Bigg[E_M\big(\hat{\tau},\hat{a};\hat{f},\rho\big)\Big/\sum_{k=1}^{M-1}E_k\big(\hat{\tau},\hat{a};\hat{f},\rho\big)\Bigg]. \quad (14)$$

Because the mismatch parameters $\sigma(\hat{\tau}), \sigma(\hat{a})$ and $\sigma\big(\hat{f}\big)$ defined in Eqs. (9) and (11) are determined by the statistical characteristics of the differences among channels, the same mismatch parameters always correspond to several different cases in a multiple channel system. Therefore, a statistical expectation would be a reliable method to derive an estimate for all cases with the same parameters. In other words, to derive the relation between the spectrum extinction ratio and the mismatch parameters, all the values of η in different cases corresponding to the same mismatch parameters are summarized for an average (i.e. statistical expectation). Based on this statistical method, effects of channel mismatch on the spectrum extinction ratio can be characterized by the relation between the calculated statistical expectation and mismatch parameters.

In mathematics, the calculation of the statistical expectation can be taken as an integral over a mathematical set of mismatch cases corresponding to certain mismatch parameters.

Without loss of generality, a space of x is used to denote the normalized time skew $\hat{\tau}$, the normalized amplitude $\hat{a}$, or the normalized cutoff frequency $\hat{f}$. In the space of $x = (x_1, x_2,\ldots, x_M)^{\mathrm{T}}$, a mathematical set of mismatch parameter $\sigma(x)$ can be expressed as:

$$S(x): \sum_{k=1}^{M} x_k^2 = M\sigma^2(x) \text{ and } \sum_{k=1}^{M} x_k = 0. \tag{15}$$

where $S(x)$ is a (M-2) dimension sphere in the space of $x = (x_1, x_2,\ldots, x_M)^{\mathrm{T}}$ and M is the channel number. The integral over $S(x)$ can be calculated numerically as an (M-2) dimension spherical integral, which is described in details in Appendix 2. Therefore, the statistical expectation of η as a multivariate function $\eta\left[\sigma(\hat{\tau}),\sigma(\hat{a});\sigma(\hat{f}),\rho\right]$ can be derived by tripling the integral over the spheres $S(\hat{\tau})$, $S(\hat{a})$ and $S(\hat{f})$, which is expressed as follows:

$$\eta\left[\sigma(\hat{\tau}),\sigma(\hat{a});\sigma(\hat{f}),\rho\right] = \frac{\iiint \eta\left(\hat{\tau},\hat{a};\hat{f},\rho\right) dS(\hat{\tau})\,dS(\hat{a})\,dS(\hat{f})}{\int dS(\hat{\tau})\int dS(\hat{a})\int dS(\hat{f})}. \tag{16}$$

Note that the pulse shape mismatch cannot be compensated in the experiment configuration shown in Fig. 1(a). Therefore the spectrum extinction ratio η is limited by the pulse shape mismatch, which can be denoted by the spectrum extinction ratio without mismatches in clock timing and amplitude as follows

$$\eta\left[\sigma(\hat{f}),\rho\right] = \int \eta\left(0,0;\hat{f},\rho\right) dS(\hat{f}) \Big/ \int dS(\hat{f}). \tag{17}$$

For a certain pulse shape, normalized cutoff frequency $\hat{f}_k$ and normalized frequency ratio ρ are constants determined by Eqs. (11) and (12), respectively. The relation between spectrum extinction ratio η and clock timing mismatch and amplitude mismatch with a certain pulse shape mismatch can be expressed as follows

$$\eta\left[\sigma(\hat{\tau}),\sigma(\hat{a})\right] = \iint \eta\left(\hat{\tau},\hat{a};\hat{f},\rho\right) dS(\hat{\tau})\,dS(\hat{a}) \Big/ \iint dS(\hat{\tau})\,dS(\hat{a}). \tag{18}$$

3.3 Explicit analysis of 2-channel model

As a simple example, we demonstrate an explicit analysis of the differences between two pulse trains. The impacts of channel mismatch effects are shown in Fig. 3. The spectrum extinction ratio η can be drawn intuitively from the amplitude difference between two spectrum peaks ($f_s/2$ and f_s). A schematic of the ideal clock and simulated RF spectrum is illustrated in Fig. 3(a). The cases with only one of the mismatch effect of clock timing mismatch, amplitude mismatch, or pulse shape mismatch is shown in Figs. 3(b)-3(d), respectively. In the simulations, the noise is modeled as a complex Gaussian distribution and the power spectral density (PSD) of noise is taken to be 10^{-17} mW/Hz for consistence with the experimental measurement as present below. Note that our simulation results are not sensitive to the exact noise distribution so that this noise PSD is applied to all following simulations.
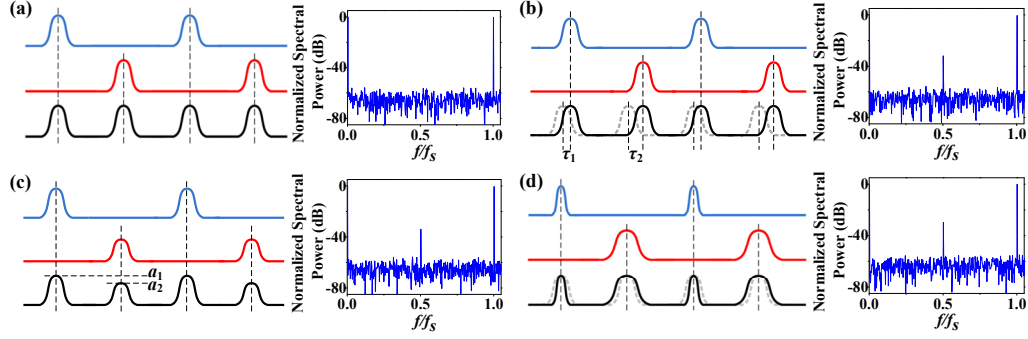
Fig. 3. Schematic of pulse train mismatch (left) and the corresponding RF spectrum (right). Sampling rate f_s = 40GHz. (a) Ideal clock. (b) Clock timing mismatch only. τ_1 = −0.2ps and τ_2 = 0.2ps. (c) Amplitude mismatch only. a_1 = 1.01 and a_2 = 0.99. (d) Pulse shape mismatch only. $f_{c,1}$ = 73.66GHz and $f_{c,2}$ = 69.06GHz.

Taking into account all the mismatch parameters, the explicit expressions of E_s and E_n for $M = 2$ can be derived from Eq. (13) as follows

$$E_s = \left(R_{\mathrm{PD}}\bar{a}/2T_s\right)^2 \left| u_2\left[\sigma\left(\hat{f}\right),\rho\right]\left[1+\sigma\left(\hat{a}\right)\right]e^{-j2\pi\sigma\left(\hat{\tau}\right)} + u_2\left[-\sigma\left(\hat{f}\right),\rho\right]\left[1-\sigma\left(\hat{a}\right)\right]e^{j2\pi\sigma\left(\hat{\tau}\right)} \right|^2 .$$

$$E_n = \left(R_{\mathrm{PD}}\bar{a}/2T_s\right)^2 \left| u_1\left[\sigma\left(\hat{f}\right),\rho\right]\left[1+\sigma\left(\hat{a}\right)\right]e^{-j\pi\sigma\left(\hat{\tau}\right)} - u_1\left[-\sigma\left(\hat{f}\right),\rho\right]\left[1-\sigma\left(\hat{a}\right)\right]e^{j\pi\sigma\left(\hat{\tau}\right)} \right|^2$$

(19)

The corresponding explicit expression of spectrum extinction ratio η can be derived from Eq. (6) as a multivariate function $\eta = \eta\left[\sigma(\hat{\tau}),\sigma(\hat{a});\sigma(\hat{f}),\rho\right]$. For a more explicit analysis and the simplicity of expressions, the analysis is carried out for two different cases: only clock timing and amplitude mismatch; only pulse shape mismatch, respectively. With only clock timing and amplitude mismatches, the expression of η can be expressed as

$$\eta\left[\sigma(\hat{\tau}),\sigma(\hat{a});0,0\right] = 10\log_{10}\left[\frac{2-\left[1-\sigma^2\left(\hat{a}\right)\right]\left[1-\cos 4\pi\sigma\left(\hat{\tau}\right)\right]}{2\sigma^2\left(\hat{a}\right)+\left[1-\sigma^2\left(\hat{a}\right)\right]\left[1-\cos 2\pi\sigma\left(\hat{\tau}\right)\right]}\right]. \quad (20)$$

With only pulse shape mismatches, the expression of η can be written as

$$\eta\left[0,0;\sigma\left(\hat{f}\right),\rho\right] = 10\log_{10}\frac{\left|u_2\left[\sigma\left(\hat{f}\right),\rho\right]+u_2\left[-\sigma\left(\hat{f}\right),\rho\right]\right|^2}{\left|u_1\left[\sigma\left(\hat{f}\right),\rho\right]-u_1\left[-\sigma\left(\hat{f}\right),\rho\right]\right|^2}. \quad (21)$$

Simulation of Eqs. (20) and (21) are depitcted in Figs. 4(a) and 4(b), respectively. It is shown that the spectrum extinction ratio η decreases as mismatch parameters increase. In comparison, the impact of clock timing and amplitude mismatch is much more serious than that of pulse shape mismatch provided the same value of mismatch parameters.
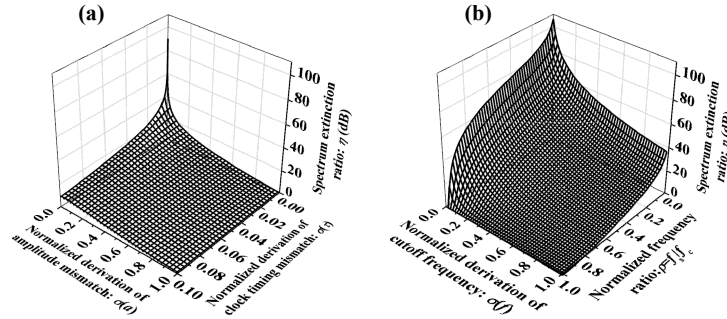
Fig. 4. Spectrum extinction ratio versus (a) only clock timing and amplitude mismatch and (b) only pulse shape mismatch ($M = 2$).

4. Experiment and discussion

In the experiment, the mode-locked laser source is an actively mode locked fiber laser with a repetition rate at 10 GHz (Calmar PSL-10-TT), which is compressed by a pulse compressor (Calmar PCS-2). The output spectrum from the source is sliced into 4 channels by a WDM, which is precisely detuned in power and time via VOAs and TDLs to generate a time-wavelength interleaved clock at the repetition rate of $f_s = 40$GHz. The optical spectra of all channels are measured by an optical spectrum analyzer (Yokogawa AQ6370C) as shown in Fig. 5(a). The central wavelengths are 1546.92nm, 1548.51nm, 1553.33nm, and 1554.94nm, respectively. The spectrum width of each channel is much smaller than the output spectrum width of the mode locked laser. WDM, TDLs, and VOAs are all passive components which do not induce the additional phase fluctuations. Therefore, the phase fluctuation of the pulse shape in each channel should be small enough and ignorable, which means an inverted Fourier transform can be used to deduce the corresponding temporal pulse shape from the optical spectrum. Figure 5(b) depicts the deduced temporal pulse shapes which are normalized to their average amplitudes. The normalized amplitude $\hat{a}_k$ can be derived from the amplitudes of temporal pulse shapes (see Fig. 5(b)) and the results are summarized in Table 1.

For the calculation of pulse shape mismatch, Fig. 6(a) shows the normalized temporal pulse shapes $u_k(t)$ in all 4 channels. $\tilde{u}_k(f)$ in each channel is calculated by Fourier transform of $u_k(t)$ and illustrated in Fig. 6(b). With $\tilde{u}_k(f)$ in each channel, the normalized cutoff frequencies $\hat{f}_k$ are calculated by Eq. (11) and also summarized in Table 1.
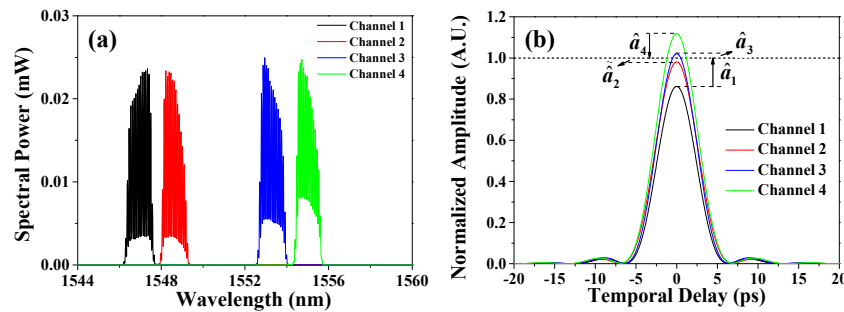

Fig. 5. (a) Measured optical spectrum in each channel and (b) temporal pulse shapes normalized to the average amplitude for the calculation of normalized amplitude $\hat{a}_k$.
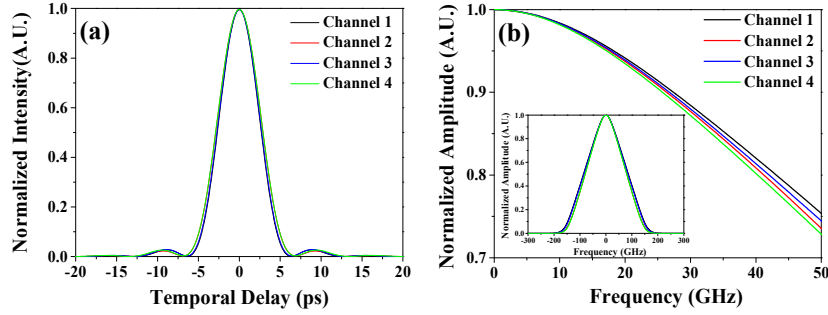
Fig. 6. (a) Normalized temporal pulse shapes and (b) $\tilde{u}_k(f)$ of all 4 channels. The inset in (b) is a full-scale plot.

With a 100-GHz photo-detector (U2t XPDV4120R), the RF spectrum with certain values of TDLs and VOAs is measured by a RF spectrum analyzer (R&S FSUP50) and shown in Fig. 7(a). The normalized time skews $\hat{\tau}_k$ can be solved from the following equations derived from Eq. (13):

$$\begin{cases} 10\log_{10}\dfrac{E_4\left(\hat{\tau},\hat{a};\hat{f},\rho\right)}{E_k\left(\hat{\tau},\hat{a};\hat{f},\rho\right)}=P(4)-P(k) \quad k=1,2,3 \\ \displaystyle\sum_{k=1}^{4}\hat{\tau}_k=0 \end{cases} \tag{22}$$

where the normalized amplitude $\hat{a}_k$ and normalized cutoff frequency $\hat{f}_k$ are shown in Table 1, the normalized frequency ratio ρ can be calculated by Eq. (12), and $P(k)$ is the power at $f = kf_s/M$ in unit of dBm (see Fig. 7(a)).

Table 1. Normalized amplitude, time skew and cutoff frequencies of all 4 channels evaluated from experimental data.

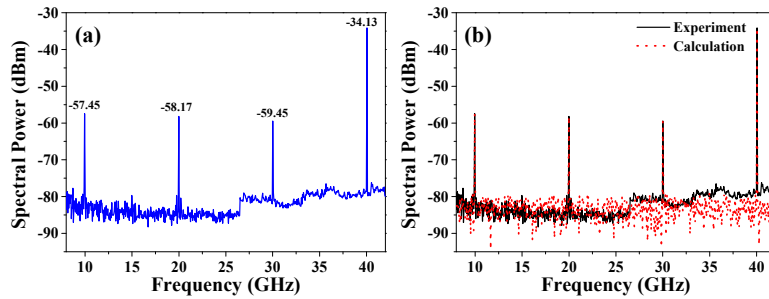| Channel	1	2	3	4
$\hat{a}_k$	−0.133	−0.014	0.025	0.122
$\hat{f}_k$	0.0348	−0.0173	0.0071	−0.0245
$\hat{\tau}_k$	−0.0082	−0.0093	0.0169	0.0006

Fig. 7. (a) RF spectrum measured by R&S FSUP50 spectrum analyzer, (b) Comparison of the calculated and measured RF spectra.

In order to avoid multiple solutions, the values of normalized time skew $\hat{\tau}_k$ are restricted within the interval of [-0.5, 0.5]. Equation (22) is solved numerically and thus the mismatch

parameters of $\hat{\tau}_k$ are calculated, which are also summarized in Table 1. Figure 7(b) compares the solution of the RF spectrum calculated by Eq. (13) with the experimental measurement, showing good consistence. With the values of $\hat{a}_k$ and $\hat{\tau}_k$ extracted from experiment measurement, the mismatch parameter of clock timing mismatch and amplitude mismatch are respectively deduced to be $\sigma(\hat{\tau}) = 0.0044$ and $\sigma(\hat{a}) = 0.092$.

Referred to Table 1, proper adjustments are applied to the TDLs and VOAs among all 4 channels so as to compensate the channel mismatches. The measured and calculated RF spectra after each-step adjustment are shown in Figs. 8(a)-8(d), respectively. The corresponding mismatch parameters and spectrum extinction ratios after four-step adjustments are summarized in Table 2. The results illustrate that the measured and expected spectrum extinction ratios (η) increase from 19.38dB to 34.68dB after adjustments. By use of the parameters $\hat{f}_k$ from Table 1, the dependence of η as a function of the timing and amplitude mismatches is estimated by Eq. (18), which is depicted in Fig. 9(a).

Figure 9(b) compares both experimental and theoretical analysis. The values in the brackets and denoted by pentangle are the values of η calculated from measured data and the curves are contours of the analytical model shown in Fig. 9(a).The values extracted from experiment after each adjustment agrees well with the expected ones which are derived from the analytical model. It validates the effectiveness of the analytical model for estimation of channel mismatch effects. The mathematical universality in multi-channel analysis of the analytical model indicates that it should be feasible for spectrum slicing based time-wavelength interleaved optical clock generation systems with more channels and higher speed, which is now under plan to further study. Each adjustment gets closer to the coordinate origin where the spectrum extinction ratio is $\eta(0,0) = 50.473$dB, which verifies the feasibility of the analytical model for compensation of channel mismatches. Note that the coordinate origin of Fig. 9(b) denotes that there is no mismatch in both amplitude and clock timing (i.e. $\sigma(\hat{\tau}) = 0$ and $\sigma(\hat{a}) = 0$) and $\eta(0,0)$ represents the limitation of the spectrum extinction ratio since the pulse shape mismatch cannot be compensated yet. However, this limitation is not successfully achieved due to the limited accuracy of TDL and VOA used in our experimental configuration.
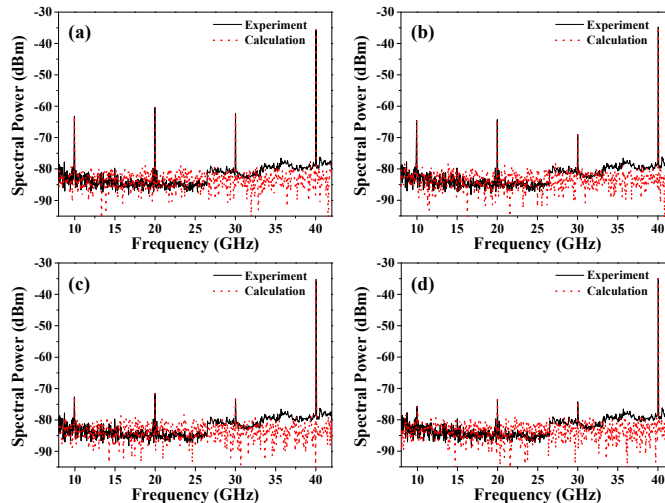

Fig. 8. (a)-(d): Comparison of simulated and measured RF spectrum after four adjustments of TDLs and VOAs.

Table 2. Mismatch parameters and spectrum extinction ratios after each adjustment.

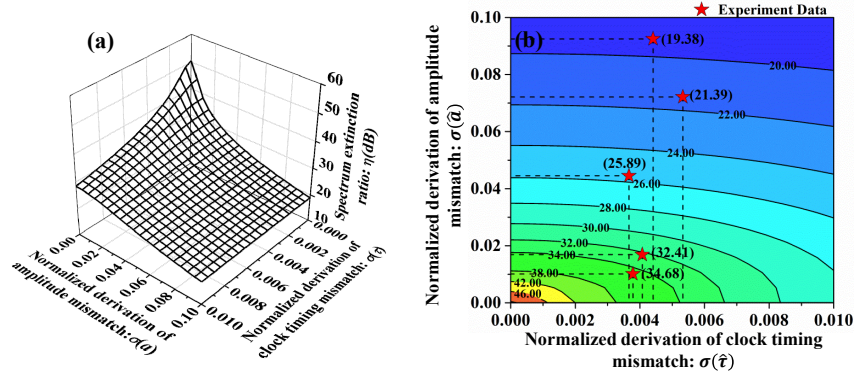| Adjustment	0	1	2	3	4
$\sigma(\hat{\tau})$	0.0044	0.0053	0.0037	0.0041	0.0038
$\sigma(\hat{a})$	0.092	0.072	0.044	0.017	0.010
η (measured)/dB	19.38	21.39	25.89	32.41	34.68
η (expected)/dB	19.40	21.36	26.02	32.40	34.68

Fig. 9. (a) Dependence of spectrum extinction ratio on the timing and amplitude mismatches deduced from the experimental measurement ($M = 4$). (b) The contour of the surface in (a). Solid curves: theoretical analysis. Pentangle: the experimental measurement.

5. Conclusion

We have demonstrated a frequency domain scheme of channel mismatch measurement and compensation for high speed time-wavelength interleaved optical clock based on spectrum slicing of mode locked fiber laser. An analytical model of the relation between channel mismatch effects and spectrum measurement is established to estimate the channel mismatches effects of clock timing, amplitude, and pulse shape. Based on the analytical model, an explicit analysis is carried out for a 2-channel model and a 4-channel channel model. For validation of our analytical model, we set up a 4-channel time-wavelength interleaving experiment configuration which generates a 40 GHz optical clock via spectrum slicing of a 10 GHz mode-locked fiber laser. The feasibility of the analytical model in multi-channel mismatch analysis has been validated through the comparison with data extracted from the experiment configuration. The analytical model should be effective for the mismatch analysis in the time-wavelength interleaving system with more channels and higher speed.

Appendix 1: Lorentz approximation of $\tilde{u}(f)$

The Lorentz approximation is applied to the Fourier transform of the temporal pulse shape in Section 3.1 to characterize the pulse shape mismatch. This approximation is derived by Taylor expansion of $1/\tilde{u}(f)$ as follows:

$$1/\tilde{u}(f) \approx c_0 + c_1 f + c_2 f^2 + \text{c.c.} \tag{23}$$

$1/\tilde{u}(f)$ gets its minimum at $f=0$ so that $c_1 = \delta(1/\tilde{u})/\delta f \big|_{f=0} = 0$. Hence the approximation in Eq. (23) becomes a linear approximation of f^2:

$$1/\tilde{u}(f) \propto 1 + (f/f_c)^2, \quad 1/f_c^2 = \delta(1/\tilde{u})/\delta(f^2)\big|_{f=0}. \tag{24}$$

Since the sampling rate f_s is much smaller than optical spectrum width, the coefficient of f_c can be calculated at $f = f_s$ as an approximation of $f=0$, which can be expressed:

$$f_c^2 = \left[\delta\left(1/\tilde{u}\right)\big/\delta\left(f^2\right)\right]^{-1}\bigg|_{f=0} \approx \left[\delta\left(1/\tilde{u}\right)\big/\delta\left(f^2\right)\right]^{-1}\bigg|_{f=f_s} = -2f_s\tilde{u}^2\left(f_s\right)\big/\tilde{u}'\left(f_s\right) \quad (25)$$

With Eqs. (24) and (25), the approximation in Eq. (10) is derived.

Appendix 2: Calculation of sphere integral

The integral in Eq. (16) can be calculated by tripling the integral on the sphere in Eq. (15). For the calculation of the integral, we consider an integral of the function $\eta(x)$ on a (M-2) dimension sphere $S(x)$ ($M>2$) in the space of $x=(x_1,x_2,\dots,x_M)^{\mathrm{T}}$ as follows:

$$I = \int \eta(x)\,dS(x) . \quad (26)$$

Note that the expression of the sphere in Eq. (15) is not explicit for the calculation in the coordinates $x=(x_1,x_2,\dots,x_M)^{\mathrm{T}}$, so that a unitary orthogonal matrix $\mathbf{A}$ is demanded to transform the coordinates $x=(x_1,x_2,\dots,x_M)^{\mathrm{T}}$ into $u=(u_1,u_2,\dots,u_M)^{\mathrm{T}}$ as

$$u = \mathbf{A}x, \, x = \mathbf{A}^T u . \quad (27)$$

In the new coordinates $u=(u_1,u_2,\dots,u_M)^{\mathrm{T}}$, the sphere $S(x)$ should be derived into a standard sphere expression $S(u)$ as follows

$$S(u): \sum_{k=2}^{M} u_k^2 = M\sigma^2(x), \text{ and } u_1 = 0. \quad (28)$$

To obtain the transform matrix $\mathbf{A}$, the expression of the basis vectors in the new coordinates should be derived first. Note that the normalized law vector of the plane, where sphere $S(x)$ is included, is $1/\sqrt{M}\,(1,1,\dots,1)^T$. Setting this vector as the basis vector corresponding to u_1, a normalized base of the new coordinates can be derived as

$$\begin{aligned}
\mathbf{v}_1 &= \left(1/\sqrt{M}\right)(1,1,\cdots,1,1)^T \\
\mathbf{v}_2 &= \left(1/\sqrt{2}\right)(1,0,\cdots,0,-1)^T \\
\mathbf{v}_3 &= \left(1/\sqrt{2}\right)(0,1,\cdots,0,-1)^T . \\
&\quad\vdots \\
\mathbf{v}_M &= \left(1/\sqrt{2}\right)(0,0,\cdots,1,-1)^T
\end{aligned} \quad (29)$$

The base of Eq. (29) is not orthogonal. Therefore, a Schmidt-Gram method is applied to orthogonalize this base as follows

$$\begin{aligned}
\mathbf{e}_1 &= \mathbf{v}_1 \\
\mathbf{e}_2 &= \mathbf{v}_2 - \left(\mathbf{v}_2 \cdot \mathbf{e}_1\right)\mathbf{e}_1 \\
\mathbf{e}_3 &= \mathbf{v}_3 - \left(\mathbf{v}_3 \cdot \mathbf{e}_1\right)\mathbf{e}_1 - \left(\mathbf{v}_3 \cdot \mathbf{e}_2\right)\mathbf{e}_2 . \\
&\quad\vdots \\
\mathbf{e}_M &= \mathbf{v}_M - \sum_{k=1}^{M-1}\left(\mathbf{v}_M \cdot \mathbf{e}_k\right)\mathbf{e}_k
\end{aligned} \quad (30)$$

With the base of new coordinates derived as Eq. (30), the transform matrix $\mathbf{A}$ can be expressed as

$$\mathbf{A} = \left(\mathbf{e}_1, \mathbf{e}_2, \cdots, \mathbf{e}_{M-1}, \mathbf{e}_M\right). \quad (31)$$

In the space of $u = (u_1, u_2, \ldots, u_M)^\mathrm{T}$, the integral can be calculated explicitly via a sphere coordinates transform $u = u(R, \varphi_1, \varphi_2, \ldots, \varphi_{M-2})$ as follows

$$
\begin{aligned}
u_1 &= 0 \\
u_2 &= R\cos\varphi_1 \\
u_3 &= R\sin\varphi_1\cos\varphi_2 \\
&\;\;\vdots \\
u_{M-1} &= R\sin\varphi_1\sin\varphi_2\cdots\sin\varphi_{M-3}\cos\varphi_{M-2} \\
u_M &= R\sin\varphi_1\sin\varphi_2\cdots\sin\varphi_{M-3}\sin\varphi_{M-2}
\end{aligned}
\qquad (32)
$$

where $R = \sqrt{M}\,\sigma(x)$, $\varphi_k \in [0,\pi]$, $k = 1,2,\ldots,M\text{-}3$, $\varphi_{M-2} \in [0,2\pi]$. With the sphere coordinates transform, the differential area could be taken as

$$
\mathrm{d}S\big[u(R,\varphi_1,\varphi_2,\cdots,\varphi_{M-2})\big] = R^{M-2}\prod_{k=1}^{M-3}\sin^{(M-2)-k}\varphi_k\prod_{k=1}^{M-2}\mathrm{d}\varphi_k. \qquad (33)
$$

Hence the integral in Eq. (26) can be calculated numerically as

$$
I = \int_0^{2\pi}\cdots\int_0^{\pi}\int_0^{\pi}\eta\big[\mathbf{A}^T u(R,\varphi_1,\varphi_2,\cdots,\varphi_{M-2})\big]\mathrm{d}S\big[u(R,\varphi_1,\varphi_2,\cdots,\varphi_{M-2})\big]. \qquad (34)
$$

The area of (M-2) dimension sphere gives that

$$
\int \mathrm{d}S = \int_0^{2\pi}\cdots\int_0^{\pi}\int_0^{\pi}R^{M-2}\prod_{k=1}^{M-3}\sin^{(M-2)-k}\varphi_k\prod_{k=1}^{M-2}\mathrm{d}\varphi_k = \frac{2\pi^{(M-1)/2}R^{M-2}}{\Gamma\big[(M-1)/2\big]}, \qquad (35)
$$

where $\Gamma(\cdot)$ is gamma function. With Eqs. (34) and (35), the integral in Eq. (26) could be calculated numerically.

For the calculation of M=2 case, the integral in Eq. (26) degenerates into a sum of two points $[\sigma(x), -\sigma(x)]$ and $[-\sigma(x), \sigma(x)]$ as follows

$$
I = \eta\big\{[\sigma(x), -\sigma(x)]\big\} + \eta\big\{[-\sigma(x), \sigma(x)]\big\}. \qquad (36)
$$

Note that the explicit analysis of 2-channel case in Eqs. (19)-(21) is based on Eq. (36).

Acknowledgment